PAPER

Studies of the weak interaction in atomic systems: towards measurements of atomic parity non-conservation in francium

To cite this article: G Gwinner and L A Orozco 2022 *Quantum Sci. Technol.* **7** 024001

Quantum Science and Technology

PAPER

Studies of the weak interaction in atomic systems: towards measurements of atomic parity non-conservation in francium

RECEIVED
2 September 2021

REVISED
2 December 2021

ACCEPTED FOR PUBLICATION
17 December 2021

PUBLISHED
21 January 2022

G Gwinner[1,*] and L A Orozco[2]

[1] Department of Physics and Astronomy, University of Manitoba, Winnipeg, Manitoba, R3T 2N2, Canada
[2] Joint Quantum Institute, Department of Physics, University of Maryland, College Park, MD 20742, United States of America
[*] Author to whom any correspondence should be addressed.

E-mail: Gerald.Gwinner@umanitoba.ca

Keywords: precision measurements, weak interactions, quantum science and technology, atomic parity non-conservation

Abstract

Tests of the standard model of particle physics should be carried out over the widest possible range of energies. Here we present our plans and progress for an atomic parity non-conservation experiment using the heaviest alkali, francium ($Z = 87$), which has no stable isotope. Low-energy tests of this kind have sensitivity complementary to higher energy searches, e.g. at the large hadron collider.

1. Introduction

Parity non-conservation (PNC) is a unique signature of the weak interaction. The weak interaction mixes states of opposite parity and produces two types of atomic PNC (APNC) effects in atoms: nuclear spin independent (nsi) and nuclear spin dependent (nsd) [1]. All past and on-going APNC experiments rely on the large enhancement of the observed effect in heavy nuclei (large Z), first pointed out by the Bouchiats [2–4]. Francium, the heaviest alkali atom ($Z = 87$), has received much attention in recent years [5]. It possesses a unique combination of structural simplicity thanks to its single valence s-electron and a great sensitivity to effects such as APNC and possible permanent electric dipole moments (EDM) due to its high nuclear charge. Our knowledge of Fr has, however, been limited due to the fact that it is the least stable element among the first 103 of the periodic table; its longest lived isotope, ^{223}Fr, has a half-life of only 23 min.

The attractiveness of Fr for APNC experiments has been discussed since the early 1990s in the context of searches for 'new' physics beyond the standard model (SM) [5–8]. APNC arises from the parity-violating exchange of Z-bosons between electrons and the quarks in the nucleus, leading to a mixing of atomic levels of opposite parity [2]. As a result, otherwise strictly forbidden electric dipole transitions can be excited between states of the same parity. APNC was first observed in the late 1970s [9, 10] (for an overview, see [11]). The culmination so far has been a measurement by Wieman's group in Boulder in ^{133}Cs [12]. APNC scales with the nuclear charge roughly as Z^3, favoring experiments in heavy atoms, but a successful extraction of the weak interaction physics from the measured atomic quantity also requires a detailed understanding of the atomic wavefunctions and some nuclear properties. This has limited the interpretation of Tl, Pb, and Bi data. The atomic theory of Fr, on the other hand, can be understood at a level similar to that of Cs ($Z = 55$), yet the APNC effect is almost 20 times larger [13, 14].

2. Precision measurements in the context of quantum technologies

The quantum states in atoms and more generally in molecules open exciting frontiers in precision measurement science. They can serve as a suite of potential clocks, and as exquisite sensors for new physics. They can provide a window into discrete symmetry violations and physics beyond the SM [15, 16].

It is the possibility of interference, at the heart of quantum mechanics, that becomes the natural amplifier for these effects. The further ability to control quantum noise is quickly becoming the focus of the precision measurement [17, 18] and the quantum information communities.

In the case of APNC, one interferes the exceedingly small parity non-conserving amplitude $A_{\rm PNC}$ (which by itself would give rise to a transition of oscillator strength $f \approx 10^{-22}$ in Cs) with a much larger parity conserving amplitude $A_{\rm PC}$,

$$|A_{\rm PC} + A_{\rm PNC}|^2 = |A_{\rm PC}|^2 + 2\,{\rm Re}(A_{\rm PC}A^*_{\rm PNC}) + |A_{\rm PNC}|^2. \quad (1)$$

The interference term is then amplified relative to $|A_{\rm PNC}|^2$ by the factor $|A_{\rm PC}/A_{\rm PNC}|$, e.g. $\approx 10^6$ in the Cs experiment. Most crucially, as the interference term is linear in $A_{\rm PNC}$, it changes sign under parity transformations, which allows us to extract the weak interaction signature in the presence of much larger background signals. This motivates experimental geometries with several handedness reversals for redundancy.

3. APNC and the standard model

APNC has played an important role in uncovering the neutral current weak interaction. Shortly after the landmark e-D inelastic scattering experiment at SLAC [19] measured the parity violating part of the neutral current weak interaction, APNC confirmed these findings at a very different momentum scale. In terms of the parity-violating electron–quark coupling constants C_{1u} and C_{1d}, APNC provides complementary constraints compared to parity-violating electron scattering (PVES), as demonstrated in figure 1. Only together can they determine the individual couplings to the down and up quarks (or alternatively, proton and neutron). Even (in fact *more so*) in the large hadron collider (LHC) era, low energy experiments have a key role to play. For example, when new states are discovered at the LHC, it will be important to know their couplings to the first generation of particles [20]. Electrons and muons can be distinguished in the LHC detectors, but up/down quark jets cannot be separated from jets of other generations. APNC and other low-energy experiments are in a unique position to assist with this question. APNC measures the strength of the weak neutral current at very low momentum transfer. There are three types of such 'low-energy' weak neutral current measurements with complementary sensitivity. The atomic weak charge is predominantly sensitive to that of the neutron, due to the proton's near-vanishing weak charge, proportional to $(1{-}4\sin^2\theta_{\rm W})$, where $\theta_{\rm W}$ is the *Weinberg* or *weak* angle. The Qweak electron scattering experiment on hydrogen is sensitive to the proton's weak charge. E158 at SLAC and the upcoming MOLLER experiment at JLab measure electron–electron Møller scattering and are thus sensitive to the electron's weak charge. Different SM extensions then contribute differently [22]. The atomic weak charge is relatively insensitive to one-loop order corrections from all SUSY particles, hence its measurement provides a benchmark for possible departures by the other low-energy observables. Møller scattering is purely leptonic and has no sensitivity to leptoquarks, and APNC can provide the sensitivity to those. Figure 2 shows results for the Weinberg angle as a function of momentum transferred, Q. The low-energy experiments have competitive sensitivity to certain specific SM extensions compared to the collider electroweak measurements—the latter's precision is better, but the low-energy experiments seeking terms interfering with the Z exchange can have inherently more sensitivity to tree-level exchange because they work on the tail of the Z resonance. It should be stressed that figure 2 cannot do justice to the highly complementary nature of the low-energy experiments, as it only plots the sensitivity to one SM parameter, $\sin^2\theta_{\rm W}$. Since Qweak and APNC probe different quark combinations and E158/MØLLER probe leptons, the sensitivities to physics beyond the SM are very different.

Many SM extensions consider exchange bosons with electroweak coupling strength whose low-energy interactions are reduced by their heavier masses. In contrast, $g-2$ of the muon [25] as well as many astro-particle phenomena (511 keV radiation, high-energy positrons) [27] are modelled by interactions with much lighter exchange bosons with 'unnatural', small, intrinsic couplings. APNC results tightly constrain such interactions to conserve parity.

In addition to the leading-order nsi APNC effect (i.e. an axial electron current interaction with a nuclear vector current, $A_{\rm e}V_{\rm N}$) discussed above, nsd APNC was unambiguously observed in the Boulder Cs experiment for the first time by extracting the dependence of APNC on the hyperfine (hf) levels involved, and hence nuclear spin. Several effects contribute to this part, but in heavy atoms the nuclear anapole moment dominates, which is a parity non-conserving, time reversal conserving moment that arises from weak interactions between the nucleons [28–30]. This has opened up the possibility to study weak nucleon–nucleon interactions via precise atomic spectroscopy. In Fr, the anapole effect is predicted to be one order of magnitude larger than in Cs. Fr is nearer to a closed nuclear shell and with nuclear structure

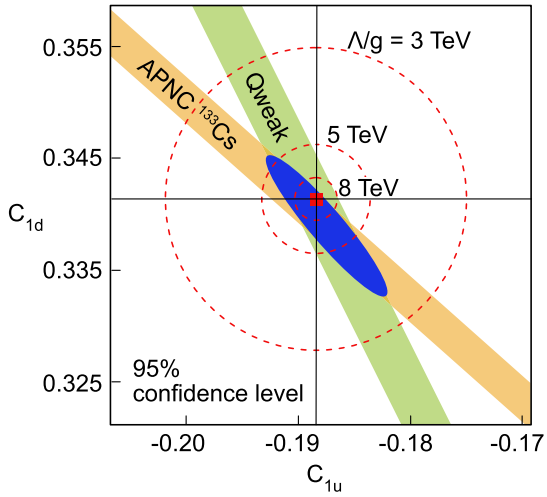

Figure 1. Constraints on parity-violating, weak electron–quark couplings from electron scattering and APNC, showing their complementarity; the red dot is the SM prediction, dashed circles show the remarkable sensitivity for 'new' physics at mass scales Λ/g. Plot generated from data provided in [21].

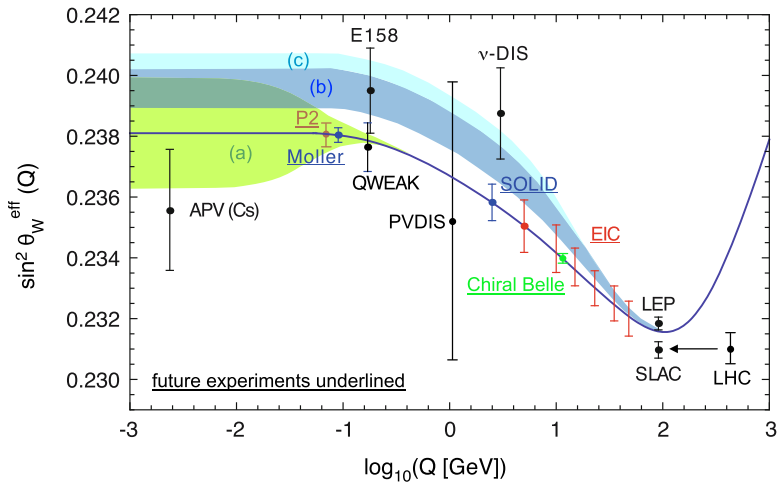

Figure 2. Past and future measurements of the Weinberg angle. Data points for future experiments are arbitrarily centered on the SM prediction (solid black line). Reproduced from [23]. CC BY 4.0. Chiral Belle from [24]. Scenarios with dark Z bosons for m_{Z_d} of (a) 50 MeV, (b) and (c) 15 GeV (where area (c) is in tension with existing constraints) from [25, 26].

shown to be regular, for example by hf anomaly measurements [31, 32], it is an excellent candidate for anapole studies [33].

4. Atomic parity non-conservation

The exchange of weak neutral currents between electrons and nucleons constitutes the main source of parity violation in atomic transitions. The currents are of two kinds, depending on whether the electron or the nucleon enters as the axial vector current.

The Hamiltonian for an infinitely heavy nucleon without radiative corrections is [11]

$$H = \frac{G}{\sqrt{2}}(\kappa_{1i}\gamma_5 - \kappa_{\mathrm{nsd},i}\boldsymbol{\sigma}_\mathrm{n}\cdot\boldsymbol{\alpha})\,\delta(\mathbf{r}), \tag{2}$$

where G is the Fermi constant, γ_5 and α are Dirac matrices, σ_n are Pauli matrices, and κ_{1i} and $\kappa_{\mathrm{nsd},i}$ are constants of the interaction with $i = \mathrm{p},\ \mathrm{n}$ for a proton or a neutron and nsd = nuclear spin dependent. The δ-function is a manifestation of the short range of the weak interaction. The SM tree level values for the nsi constants are $\kappa_{1\mathrm{p}} = \frac{1}{2}(1 - 4\sin^2\theta_\mathrm{W})$ and $\kappa_{1\mathrm{n}} = -\frac{1}{2}$, with $\sin^2\theta_\mathrm{W} \approx 0.23$, and θ_W the Weinberg angle. In an atom, the contribution from equation (2) for all the nucleons must be added. For the nsi part, we obtain for

a nucleus with Z protons and N neutrons

$$H_{\mathrm{PNC}}^{\mathrm{nsi}} = \frac{G}{\sqrt{2}}\frac{Q_{\mathrm{W}}}{2}\gamma_5\,\delta(\mathbf{r}), \tag{3}$$

where $Q_{\mathrm{W}} = 2(\kappa_{1\mathrm{p}}Z + \kappa_{1\mathrm{n}}N)$ is the *weak charge* of the atom. Because of the strong cancellation in $\kappa_{1\mathrm{p}}$, the SM value for the atom's weak charge is almost equal to $-N$. The theoretical uncertainty present in all the extractions of weak interaction parameters from APNC comes from the calculation of the atomic matrix element γ_5 [34]. Due to the dominant contribution by the neutrons, nsi APNC is sensitive to the neutron radius of the nucleus. A recent neutron radius study carefully considering correlations suggests that the fractional correction for ^{213}Fr is -0.46%, with a finite but manageable error of 0.13% [35]. The PRex/CRex experiments (neutron radii of ^{208}Pb and ^{48}Ca via PVES at Jefferson Lab) should reduce this error further.

The second term of equation (2) represents the nuclear spin dependent part nsd, and due to the pairing of nucleons, its contribution has a weaker dependence on Z. Several processes contribute, but in heavy atoms, the anapole interaction dominates. Assuming a single valence nucleon of unpaired spin, Flambaum *et al* obtained [36, 37]

$$H_{\mathrm{PNC}}^{\mathrm{nsd}} = \frac{G}{\sqrt{2}}\frac{K\boldsymbol{I}\cdot\alpha}{I(I+1)}\kappa_{\mathrm{nsd},i}\delta(\mathbf{r}), \quad \kappa_{\mathrm{nsd},i} \approx \kappa_{a,i} = \frac{9}{10}g_i\frac{\tilde{\alpha}\mu_i}{m_{\mathrm{p}}\tilde{r}_0}\mathcal{A}^{2/3}, \tag{4}$$

where $K = (I + 1/2)(-1)^{I+1/2-l}$, l is the valence nucleon orbital angular momentum, and I is the nuclear spin; $\tilde{\alpha}$ is the fine structure constant, μ_i and μ_N are the magnetic moment of the valence nucleon and of the nucleus, respectively, in nuclear magnetons, $\tilde{r}_0 = 1.2$ fm, $\mathcal{A} = Z + N$, and g_i gives the strength of the weak nucleon–nucleus potential. At the time, it was thought that $g_{\mathrm{p}} \sim 4$ and $0.2 < g_{\mathrm{n}} < 1$ [11]; now there is good experimental evidence supporting the quantum chromodynamics (QCD) expansion in $1/N_{\mathrm{c}}$ (number of colors) [38], which suppresses the isovector part, implying $g_{\mathrm{p}} \sim g_{\mathrm{n}}$. As a result, nsd APNC in heavy atoms is best suited to determine nuclear anapole moments. It arises from a number of effects, though detailed calculations suggest it is dominated by core polarization by the valence nucleons [39]. This suggestion can be tested by a systematic study of francium isotopes with paired and unpaired neutrons, especially given the observation that both magnetic dipole moments and the measurements of the next-order hf anomalies can be reproduced by similar models for the $^{207-213}$Fr isotopes with simpler nuclear structure [32]. Wood *et al* [12] measured the anapole moment of ^{133}Cs by extracting the dependence of APNC on the hf energy levels involved, and consequently nuclear spin, and the same procedure can be applied in francium. The microwave scheme proposed in [33] is currently not pursued.

5. Current status of APNC

The Boulder measurement [12, 40] in conjunction with new atomic structure calculations [34, 41] determine the weak charge Q_{w} of Cs with 0.6% accuracy, in reasonably good agreement with the SM prediction as shown in figure 2. The Budker group in Berkeley/Mainz has made a first observation of APNC in ytterbium at the 10% level followed by a study of the isotopic dependence [42, 43]. For Yb, atomic structure cannot be calculated nearly as well as in alkalis, but with help of the numerous stable isotopes available, anapole moment measurements are an obvious choice. The group at Legnaro has trapped ≈1000 Fr atoms and is planning to pursue APNC [44]. The DeMille group has made great progress towards anapole measurements in molecules [45]. Efforts with single trapped ions (Ba^+ [46] and Ra^+ [47]) are also underway. The Elliott group at Purdue is revisiting APNC in Cs using coherent control [48]. In the context of work with francium, there is also interest in francium-based searches for permanent EDMs. The Sakemi group at Tohoku University is currently setting up a francium trap for T-violation experiments [49], and a Lawrence Berkeley Lab team has produced a detailed proposal for an atomic fountain-based francium EDM experiment at TRIUMF [50].

Generally, the theory groups working on APNC-related atomic theory employ complementary techniques. Nevertheless, it is highly non-trivial to test atomic theory at this accuracy—even in Cs where many atomic observables have been measured to very high precision, such as dipole matrix elements and hf structure. A measurement in another system would be invaluable. Apart from Cs, the only atoms to which this theory can be applied while at the same time providing a sizable APNC effect are Fr, Ba^+, and Ra^+. For example, Fr has different-sized radiative corrections than cesium. Radiative correction calculations that agree in cesium differ for francium [51, 52]. This is an opportunity to choose between them and hone the best calculation to decrease the final theoretical error. Recent theoretical advances have pointed out the utility of using high-precision hf interactions in various francium states [53, 54] to constrain some classes of QED radiative corrections [55], which will lead to an improved understanding of the electron

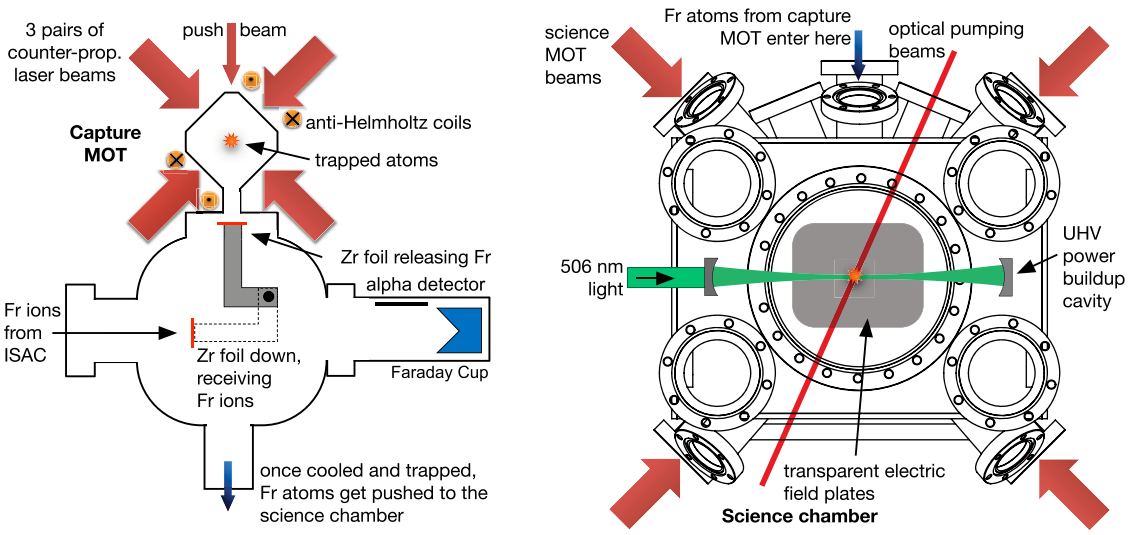

Figure 3. Layout of the FTF (not to scale). Left: capture MOT receiving Fr ions from ISAC. Once a sample is cooled and trapped, a laser push beam from the top launches the cold Fr atom cloud through a differential pumping region to the science MOT, located ≈ 70 cm below. Right: science chamber, with the main ingredients for 7*s*–8*s* spectroscopy. Not shown are the horizontal MOT beams which pass the transparent field plates, and the three-dimensional Helmholtz coil system surrounding the chamber.

wavefunction's overlap with the nucleus, a quantity of critical importance for APNC. Ultimately, the goal for a measurement of the weak charge of Fr is to match or exceed the precision of the ^{133}Cs experiment.

6. The Francium Trapping Facility

APNC experiments, and other fundamental symmetry experiments such as the searches for permanent EDMs, are challenging because the experimental signatures are very small, often at the detection limit, and superimposed on a large background. In order to observe the parity-flip induced change in fluorescence of $\approx 10^{-5}$ in the Boulder Cs APNC experiment, they used a massive thermal beam (up to 10^{15} s^{-1}cm^{-2}). Wood *et al* include a detailed discussion of their signal to noise ratio in reference [40]. With production rates of less than 10^{10} per second at any current radioactive beam facility, this is not feasible with francium. However, by using atom traps, where an individual atom can be used many times over the course of tens of seconds compared to a few μs in an atomic beam, a trapped sample of 10^6–10^7 atoms provides an equivalent scenario. With up to 10^6 Fr atoms trapped [56], we have already reached at the Francium Trapping Facility (FTF) the sample size required for a future APNC campaign envisioned to start in the near future. For the measurements leading up to APNC the number of trapped atoms is certainly sufficient. For further details about the use of laser traps with radioactive atoms see the review by Behr and Gwinner [7].

The cyclotron at TRIUMF, Canada's Accelerator Laboratory, delivers proton beams of typically several μA to a uranium carbide target unit at the Isotope Separator and Accelerator (ISAC) radioactive beam facility, producing a wide range of francium isotopes. Francium ions are transported as a low energy ion beam (20–30 keV) to the FTF, where they are deposited on a zirconium 'neutralizer' foil as shown in figure 3 on the left. The foil is about 90% of the time in the down position, intercepting Fr ions. During the remaining 10% of the time the neutralizer pivots to close the capture trap cell and is then heated to around 850°C to release the neutral Fr atoms into it. This primary trap is a vapor-cell style magneto-optical trap (MOT) with glass walls coated in silane-based dry-film to avoid the sticking of Fr (and Rb) atoms to the glass walls. The laser beams have nearly 5 cm diameter and fill the cell almost entirely, resulting in a high trapping efficiency of about 1%–2%. Keeping the trap open most of the time (a typical duty cycle is 20 s of ion collecting and 2 s of trap loading) ensures good vacuum resulting in a long trap lifetime of at least 20 s.

Once a batch of Fr atoms is trapped and cooled, a laser push beam from the top launches the atoms into the science chamber (which is located about 70 cm below the capture trap, but shown on the right in figure 3). This chamber provides an environment compatible with precision experiments: ultrahigh vacuum, low background radioactivity, and well-controlled magnetic and electric fields. A MOT in the center of the chamber re-traps the Fr atoms, and holds them in place for APNC and precursor experiments.

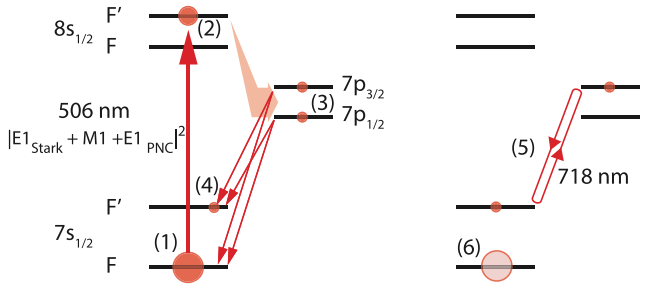

Figure 4. Relevant atomic levels of Fr, and illustration of the photon burst method used to optically amplify the 7*s*–8*s* signal. Left: at the beginning of the measuring period, all atoms are pumped e.g. into the lower hf ground state (1). After excitation to 8*s* (2) the atoms cascade down via 7*p* (3) and about half end up in the upper, depleted hf ground state (4). Right: the probe laser cycles the atom on the 7*s* F'–$7p_{3/2}$ ($F'+1$) transition (5); all atoms that were not excited to 8*s* remain 'dark' in 7*s* F (6); splittings not to scale.

7. Spectroscopy of the 7*s*–8*s* transition: toward an optical APNC experiment

The excitation $ns_{1/2} \rightarrow (n+1)s_{1/2}$ from an alkali's electronic ground state to the first excited *s*-state (see figure 4) is in the absence of external fields one of the faintest transitions observed in atoms; it is electric-dipole ($E1$) forbidden, and in the non-relativistic limit, the magnetic dipole ($M1$) amplitude also vanishes. Relativistic effects and the hf interaction with the nuclear spin give rise to an extremely weak $M1 = M1_{\rm rel} + M1_{\rm hf}$ transition with tiny oscillator strength f (10^{-15} in Cs and 10^{-13} in Fr; in contrast allowed $E1$ transitions have $f \approx 1$). Yet it is this very regime that makes the transition a compelling case for APNC measurements. Due to parity non-conserving Z-boson exchange, an additional amplitude $E1_{\rm pnc}$ exists, with a standalone oscillator strength of $\approx 10^{-21}$ in Fr, rendering it unobservable on its own. It is detected by virtue of its interference with the larger, parity-conserving amplitudes.

In the presence of an external, electric field, the transition rate R for the 7*s*–8*s* transition is

$$R_{7s-8s} \propto |E1_{\rm stark} + M1 + E1_{\rm pnc}|^2, \tag{5}$$

where $E1_{\rm stark}$ is the Stark-induced transition amplitude; a very small $E2$ amplitude stemming from off-diagonal hf mixing of *s* and *d* states has been omitted as it is not relevant for the present discussion. $E1_{\rm stark}$ can be expressed as

$$E1_{\rm stark} = \alpha \vec{E} \cdot \vec{\epsilon}\, \delta_{F,F'} \delta_{m,m'} + {\rm i}\beta (\vec{E} \times \vec{\epsilon}) \cdot \langle F' m' | \vec{\sigma} | F m \rangle, \tag{6}$$

where α and β are the scalar and vector transition polarizabilities, respectively; $\vec{E}$ is the externally applied electric field, $\vec{\epsilon}$ is the oscillating electric field of the laser radiation exciting the transition, and $\vec{\sigma}$ are the Pauli spin matrices. The total observed transition rate is the sum of the individual squared amplitudes and, importantly, the geometry and polarization dependent interference terms between them. The transition is characterized by the quantities α,β,$M1_{\rm rel}$,$M1_{\rm hf}$, and $E1_{\rm pnc}$. The ultimate goal of the APNC measurement is to determine $E1_{\rm pnc}$ and to extract the weak charge of francium from it. The other parameters are very interesting to measure in their own right, and must be determined and understood to prepare for APNC.

The parameter that needs to be determined with high precision for APNC is the vector transition polarizability β (the α term vanishes for the $\Delta F = \pm 1$ transitions used). In a Stark-interference type APNC measurement such as the Cs work done in Boulder, one measures the interference between the parity non-conserving amplitude $E1_{\rm pnc}$ and the much larger parity-conserving amplitude $E1_{\rm stark} \propto \beta E$ (for a 1 kV cm^{-1} electric field, the β Stark-induced rate exceeds the $M1$ rate by $\approx 1000\times$ and $100\times$ for Cs and Fr, respectively, and we ignore the latter in equation (7) for clarity). As in most parity violation experiments, one measures an asymmetry of the signal under parity flips. When the electric field direction is reversed, the $E1_{\rm stark}E1_{\rm pnc}$ interference term changes sign, and as a result the observed fluorescence changes. From the measured rates R_+ and R_- at opposite electric field directions, one finds the fluorescence modulation

$$\frac{R_+ - R_-}{R_+ + R_-} \propto \frac{{\rm Im}\, E1_{\rm pnc}}{\beta E}. \tag{7}$$

In essence, one determines the size of $E1_{\rm pnc}$*relative* to that of $E1_{\rm stark}$ at a known field strength E. To determine $E1_{\rm pnc}$ in absolute terms, a reliable value of β needs to be established (for Cs, see [57] and recent work in [58]). Naively, β is obtainable from $(R_+ + R_-)/2$, but unlike the ratio, the total rate depends on the number of atoms, the laser intensity, and the fluorescence detection efficiency. They cannot be calibrated to

the required sub-% precision. The solution to this conundrum arises in form of the amplitude $M1_{\rm hf}$. It can be predicted to the required precision semi-empirically from the well known, and precisely measured, hf structure. Consequently, the most crucial experiment prior to APNC will be the calibration of $E1_{\rm stark}$ against $M1_{\rm hf}$.

8. From the space sequence of the Boulder 1997 experiment to a time sequence with Fr

The Boulder experiment [40] operated with three spatial regions where the passing atomic beam was (i) prepared for the measurement, (ii) exposed to the 6*s*–7*s* radiation, and (iii) detected. Importantly, in the first and third region the magnetic field had to be transverse to the atomic beam, whereas in the second region it needed to be longitudinal. This was accomplished with an elaborate set of magnetic field coils. In between regions, the magnetic field changed direction and strength slowly enough for the Cs atoms (thermal beam velocity ≈300 m s^{-1}) to adiabatically follow.

In region 1, the atoms were optically hf and Zeeman pumped into a single state $|F, m_F\rangle$. In region 2, the atoms passed through a set of electric field plates under potential (≈700 V cm^{-1}) providing the Stark mixing, and were exposed to 6*s*–7*s* radiation enhanced by a power buildup cavity (≈ 800 kW cm^{-2}). The 6*s*–7*s* excitation and subsequent spontaneous decay via 6*p* transferred a part of the population into the other hf ground state, as illustrated for Fr in figure 4 (left panel). The presence of the triple product of the electric, magnetic, and light fields in the interaction provides the pseudoscalar quantity that modulates the 6*s*–7*s* excitation rate, and hence the population transfer, upon parity flips such as the reversal of the electric field, the magnetic field, or the light polarization.

In region 3 the atoms were interrogated using one of the two cycling transitions in the $6s_{1/2}$–$6p_{3/2}$ system, as shown for Fr in figure 4 (right panel). For each atom transferred to the other hf ground state, the cycling transition produced hundreds of photons, providing nearly complete detection efficiency for a single atom's 6*s*–7*s* excitation, despite imperfect light collection and detector efficiency.

For trapped francium, this spatial preparation, excitation, detection sequence has to be converted into a temporal one. As described in section 6, francium atoms are periodically delivered from the capture MOT to the science chamber MOT. Once the atoms are recaptured and cooled, the MOT is turned off, and a rapid sequence of optical pumping, 7*s*–8*s* excitation, and burst detection unfolds while the atoms are in free fall. After about 6 ms, the atoms are retrapped and cooled for several ms before a new measurement cycle can begin. During this time, the atom cloud falls about 0.2 mm and, assuming a temperature of ≈100 μK, expands by 0.5 mm. This sequence requires the switching of the MOT's magnetic quadrupole field and three orthogonal bias field coils on sub-millisecond timescales.

After the MOT fields are off, the atoms have to be optically pumped into one of the four stretched hf ground states $|F, m_F = \pm F\rangle$. Adopting the geometry of the Cs setup by Wood *et al* [40], the magnetic field has to be perpendicular to both the electric field and the wave vector of the 7*s*–8*s* light, leaving only the vertical axis available, along which the atoms are dropped from the capture MOT, hindering the deployment of a carefully intensity-balanced counter-propagating optical pumping beam. One option is to optically pump the atoms at an angle of 22.5° against the vertical, as indicated in figure 3, with a corresponding direction of the magnetic holding field. After the atoms are optically pumped, the magnetic field will be rotated into the vertical direction within a few hundred microseconds, permitting the atoms to adiabatically follow.

The measurement is performed by letting the atoms into the mode of a high finesse power buildup cavity (<20 kW cm^{-2}), tuned to the 7*s*–8*s* transition, for about a millisecond. This intense laser field excites the atoms in a region with a coordinate system defined by the external electric and magnetic fields and the angular momentum of the photon. If an atom gets excited it will decay via the 7*p* state, and roughly half of the time ends up in the other hf ground state. This transferred fraction will modulate with parity reversals.

Finally, an intensity-balanced, counter-propagating probe beam excites the transferred atom on a $7s$–$7p_{3/2}$ cycling transition to produce a burst of photons. In neutron-deficient Fr isotopes, the ratio of hf splitting to linewidth is larger than in Cs, and one can expect up to a few thousand photons before the atoms are pumped dark due to linewidth overlap. Great care will be needed to avoid blowing the atoms out of the trap region. This step should only take ≈100 μs, ending the measurement cycle with a subsequent return of the MOT.

The fluorescence signal during re-trapping will indicate when the number of atoms in the trap has decayed to warrant loading of a fresh sample from the capture MOT. Ultimately, it will be important to maximize the 7*s*–8*s* excitation time relative to retrapping, optical pumping, and burst detection, to around 30%, mostly limited by switching magnetic fields.

Additional complications exist. For example, the intense 7*s*–8*s* light at 506 nm must be extinguished by at least a factor of 10^6 during MOT operation, as it will photo-ionize the upper MOT state, $7p_{3/2}$, leading to rapid loss of trap population. In addition, as an atom excited to 8*s* cascades down via the $7p_{3/2}$ state, it can get photo-ionized by 506 nm light (the equivalent process cannot occur in Cs). We have measured the cross section for this process [59]. As pointed out by Vieira and Wieman [60], lowering the applied electric field (leading to a reduced 7*s*–8*s* excitation rate, but increasing the parity flip asymmetry, with a practical lower limit of 120 V cm^{-1} in Fr, where the Stark-induced and $M1$ amplitudes become equal), and reducing the intensity of the 506 nm light can address this problem. They identified another challenge, namely the intense standing wave acting as a blue-detuned dipole force on the cold atoms, pushing them towards the nodes, defeating the purpose of the cavity. FM modulation at integers of the free spectral range of the cavity can create a slowly moving travelling envelope to remedy this problem.

9. Signal to noise ratio

For an ensemble of N atoms, the Stark and PNC induced parts of the signal in photons per second are:

$$S_{\mathrm{stark}} = \frac{2}{c\epsilon_0\hbar^2} I\tau(\beta E)^2\, N \qquad S_{\mathrm{pnc}} = \frac{2}{c\epsilon_0\hbar^2} I\tau 2\beta E\, \mathrm{Im}(E_{\mathrm{pnc}})N, \tag{8}$$

where β is the vector Stark polarizability, E is the dc electric field applied for Stark mixing, $\mathrm{Im}(E_{\mathrm{pnc}})$ is the parity-violating amplitude, τ is the lifetime of the upper *s*-state, and I the intensity of the 506 nm light. Assuming shot noise limited performance (all coming from the dominating Stark part of the signal), the PNC signal-to-noise ratio achieved in t seconds for francium on the $7s \rightarrow 8s$ transition is

$$(\mathrm{S/N})_{\mathrm{pnc}} = 2\sqrt{\frac{2\tau INt}{c\epsilon_0\hbar^2}}\ \mathrm{Im}(E_{\mathrm{pnc}}). \tag{9}$$

It does not depend on the details of the Stark transition, neither β nor the applied electric field E; these quantities only enter once technical noise is considered.

We can express the time t it takes to achieve a certain signal-to-noise ratio as

$$t = \frac{(\mathrm{S/N})^2_{\mathrm{pnc}}}{NR_{\mathrm{stark}}\mathcal{A}^2}, \tag{10}$$

where $R_{\mathrm{stark}} = \frac{2\tau I}{c\epsilon_0\hbar^2}(\beta E)^2$ is the Stark excitation rate per atom and $\mathcal{A} = 2\,\mathrm{Im}(E_{\mathrm{pnc}})/(\beta E)$ is the observed PNC asymmetry. As discussed earlier, photo-ionization from the $7p_{3/2}$ state is minimized by lowering the light intensity (and thereby R_{stark}), and maximizing the PNC asymmetry by reducing the electric field. At a practical value of 200 V cm^{-1}, $\mathcal{A}_{\mathrm{Fr}} = 1 \times 10^{-4}$, about 16 times larger than in Cs. The 7*s*–8*s* excitation rate R_{stark} is limited in two ways. For one, the light intensity must be kept low enough keep photo-ionization under control. In addition, we have to take into account the fact that the atoms are interrogated in a batch mode. After (re)trapping and optical pumping, they are exposed to 506 nm light for a certain amount of time t_{ex}, and then the fraction transferred into the other hf ground state is probed. To avoid saturation of the transfer mechanism, not more than on the order of 25% of the atoms should be excited to 8*s*, before probing sets in. With the need to switch magnetic fields during the sequence, t_{ex} is on the order of a millisecond or longer, hence a maximum $R_{\mathrm{stark}} \approx 250\ \mathrm{s}^{-1}$. Such a rate should be compatible with the photo-ionization constraint. Finally, using the photon burst technique, we assume a detection efficiency $\eta \approx 0.5$ (only about half of the atoms will transfer into the other hf ground state), and apply a duty factor $f \approx 0.3$ taking into account the time for atom trapping, preparation, and probing. We can then estimate the amount of beamtime, t_{beam}, required to achieve a level of accuracy:

$$t_{\mathrm{beam}} = \frac{(\mathrm{S/N})^2_{\mathrm{pnc}}}{NR_{\mathrm{stark}}\mathcal{A}^2\eta f}. \tag{11}$$

With 10^6 trapped atoms, which is within our current capabilities, a 1% measurement (S/N = 100) would take about 7 h. A 0.2% measurement with 10^7 atoms would require about 18 h. Trapping 10^7 Fr atoms should be possible with existing Fr beam delivery, but upgraded trapping lasers. Production rates are sufficient for at least five francium isotopes. Of course, it must be stressed that these estimates are based on purely statistical considerations. Studies of systematic effects will take significant additional time. In this respect it is advantageous that the proposed experiment follows the geometry used in the Boulder Cs experiment [40]. They explored in great detail all the possible combinations of electric and magnetic field misalignment, field gradients, and imperfect light polarization, which can give rise to false PNC signals. Ultimately, it is difficult to predict in quantitative detail all of the systematic problems of this measurement.

The most important tool to study and eliminate them is to have an experiment with redundancies. The proposed apparatus will have four different reversals to check for spurious signals: reversals of the electric field, the magnetic field, the light polarization, and the Zeeman sublevel.

10. Conclusions and outlook

The current state of neutral current weak interaction tests at low-energy compels us to continue to pursue an APNC experiment with laser-trapped francium at TRIUMF. There is strong motivation to provide new data in addition to the landmark Cs result. We have established a francium atom trapping facility at the ISAC radioactive beam facility. In fall 2021 we observed the $M1$ transition with an oscillator strength of $\approx 10^{-13}$, allowing us to calibrate $M1_{\mathrm{rel}}$ and β against $M1_{\mathrm{hf}}$. Subsequent implementation of the burst detection technique will give us the sensitivity to observe atomic parity violation within 3 years. A dedicated APNC campaign would follow, once multi-beam delivery at ISAC/ARIEL provides access to more beamtime.

Acknowledgments

This work would have been impossible without the dedicated efforts of many colleagues. We thank Jiehang Zhang (University of Maryland), Robert Collister, DeHart, Timothy Hucko, Michael Kossin, and Anima Sharma (University of Manitoba), John Behr, Alexandre Gorelov, Mukut Kalita, Matt Pearson, Michaël Tandecki, and Andrea Teigelhöfer (TRIUMF), Seth Aubin (William & Mary), Eduardo Gomez (San Luis Potosí), and Gene Sprouse (Stony Brook) for their invaluable contributions. This work has been supported by the Natural Sciences and Engineering Research Council (NSERC) of Canada, by the National Research Council (NRC) of Canada through TRIUMF, the National Science Foundation (NSF), the Department of Energy (DOE) of the United States, and the University of Maryland. The University of Manitoba has supported our PhD students with University of Manitoba Graduate Fellowships and the GETS and SEGS programs.

Data availability statement

No new data were created or analysed in this study.

ORCID iDs

G Gwinner https://orcid.org/0000-0002-6744-4365

References

[1] Bouchiat M-A and Bouchiat C 1997 Parity violation in atoms *Rep. Prog. Phys.* **60** 1351–96
[2] Bouchiat M A and Bouchiat C 1974 I. Parity violation induced by weak neutral currents in atomic physics *J. Phys. France* **35** 899–927
[3] Bouchiat M A and Bouchiat C C 1974 Weak neutral currents in atomic physics *Phys. Lett.* B **48** 111–4
[4] Bouchiat M A and Bouchiat C 1975 Parity violation induced by weak neutral currents in atomic physics. part II *J. Phys. France* **36** 493–509
[5] Gomez E, Orozco L A and Sprouse G D 2005 Spectroscopy with trapped francium: advances and perspectives for weak interaction studies *Rep. Prog. Phys.* **69** 79–118
[6] Marciano W J and Rosner J L 1990 Atomic parity violation as a probe of new physics *Phys. Rev. Lett.* **65** 2963–6
[7] Behr J A and Gwinner G 2009 Standard model tests with trapped radioactive atoms *J. Phys. G: Nucl. Part. Phys.* **36** 033101
[8] Davoudiasl H, Lee H S and Marciano W J 2012 Muon anomaly and dark parity violation *Phys. Rev. Lett.* **109** 031802
[9] Barkov L M and Zolotorev M S 1978 Observation of nonconservation of parity in atomic transitions *JETP Lett.* **27** 357
[10] Barkov L M and Zolotorev M S 1979 Parity violation in atomic bismuth *Phys. Lett.* B **85** 308–13
[11] Khriplovich I B 1991 *Parity Nonconservation in Atomic Phenomena* (London: Gordon and Breach)
[12] Wood C S, Bennett S C, Cho D, Masterson B P, Roberts J L, Tanner C E and Wieman C E 1997 Measurement of parity nonconservation and an anapole moment in cesium *Science* **275** 1759–63
[13] Dzuba V A, Flambaum V V and Sushkov O P 1995 Calculation of energy levels, $E1$ transition amplitudes, and parity violation in francium *Phys. Rev.* A **51** 3454–61
[14] Safronova M S and Johnson W R 2000 High-precision calculation of the parity-nonconserving amplitude in francium *Phys. Rev.* A **62** 022112
[15] DeMille D, Doyle J M and Sushkov A O 2017 Probing the frontiers of particle physics with tabletop-scale experiments *Science* **357** 990–4
[16] Safronova M S, Budker D, DeMille D, Kimball D F J, Derevianko A and Clark C W 2018 Search for new physics with atoms and molecules *Rev. Mod. Phys.* **90** 025008
[17] Tse M *et al* 2019 Quantum-enhanced advanced LIGO detectors in the era of gravitational-wave astronomy *Phys. Rev. Lett.* **123** 231107

[18] Acernese F *et al* 2019 Increasing the astrophysical reach of the Advanced Virgo detector via the application of squeezed vacuum states of light *Phys. Rev. Lett.* **123** 231108
[19] Prescott C Y *et al* 1978 Parity non-conservation in inelastic electron scattering *Phys. Lett.* B **77** 347–52
[20] Diener R, Godfrey S and Turan I 2012 Constraining extra neutral gauge bosons with atomic parity violation measurements *Phys. Rev.* D **86** 115017
[21] Androić D *et al* 2018 Precision measurement of the weak charge of the proton *Nature* **557** 207–11
[22] Ramsey-Musolf M J and Su S 2008 Low-energy precision tests of supersymmetry *Phys. Rep.* **456** 1–88
[23] Accardi A *et al* 2016 Electron–ion collider: the next QCD frontier *Eur. Phys. J.* A **52** 268
[24] Roney M 2019 Electroweak physics with polarized beams at SuperKEKB upgrade *Proc. of 29th Int. Symp. on Lepton Photon Interactions at High Energies—PoS (LeptonPhoton2019)* vol 367 p 109 https://pos.sissa.it/367/109/
[25] Davoudiasl H, Lee H S and Marciano W J 2014 Muon $g-2$, rare kaon decays, and parity violation from dark bosons *Phys. Rev.* D **89** 095006
[26] Davoudiasl H, Lee H S and Marciano W J 2015 Low Q^2 weak mixing angle measurements and rare Higgs decays *Phys. Rev.* D **92** 055005
[27] Bouchiat C and Fayet P 2005 Constraints on the parity-violating couplings of a new gauge boson *Phys. Lett.* B **608** 87–94
[28] Zel'dovich Y B 1958 Electromagnetic interaction with parity violation *Sov. Phys. JETP* **6** 1184
[29] Flambaum V V and Khriplovich I B 1980 *P*-odd nuclear forces as a source of parity nonconservation in atoms *Sov. Phys. JETP* **52** 835
[30] Haxton W C and Wieman C E 2001 Atomic parity nonconservation and nuclear anapole moments *Annu. Rev. Nucl. Part. Sci.* **51** 261–93
[31] Grossman J S, Orozco L A, Pearson M R, Simsarian J E, Sprouse G D and Zhao W Z 1999 Hyperfine anomaly measurements in francium isotopes and the radial distribution of neutrons *Phys. Rev. Lett.* **83** 935–8
[32] Zhang J *et al* 2015 Hyperfine anomalies in Fr: boundaries of the spherical single particle model *Phys. Rev. Lett.* **115** 042501
[33] Gomez E, Aubin S, Sprouse G D, Orozco L A and DeMille D P 2007 Measurement method for the nuclear anapole moment of laser-trapped alkali-metal atoms *Phys. Rev.* A **75** 033418
[34] Porsev S G, Beloy K and Derevianko A 2009 Precision determination of electroweak coupling from atomic parity violation and implications for particle physics *Phys. Rev. Lett.* **102** 181601
[35] Brown B A, Derevianko A and Flambaum V V 2009 Calculations of the neutron skin and its effect in atomic parity violation *Phys. Rev.* C **79** 035501
[36] Flambaum V V, Khriplovich I B and Sushkov O P 1984 Nuclear anapole moments *Phys. Lett.* B **146** 367
[37] Flambaum V V and Murray D W 1997 Anapole moment and nucleon weak interactions *Phys. Rev.* C **56** 1641–4
[38] Phillips D R, Samart D and Schat C 2015 Parity-violating nucleon–nucleon force in the $1/N_c$ expansion *Phys. Rev. Lett.* **114** 062301
[39] Haxton W C, Liu C P and Ramsey-Musolf M J 2002 Nuclear anapole moments *Phys. Rev.* C **65** 045502
[40] Wood C S, Bennett S C, Roberts J L, Cho D and Wieman C E 1999 Precision measurement of parity nonconservation in cesium *Can. J. Phys.* **77** 7–75
[41] Dzuba V A, Berengut J C, Flambaum V V and Roberts B 2012 Revisiting parity nonconservation in cesium *Phys. Rev. Lett.* **109** 203003
[42] Tsigutkin K, Dounas-Frazer D, Family A, Stalnaker J E, Yashchuk V V and Budker D 2009 Observation of a large atomic parity violation effect in ytterbium *Phys. Rev. Lett.* **103** 071601
[43] Antypas D, Fabricant A, Stalnaker J E, Tsigutkin K, Flambaum V V and Budker D 2019 Isotopic variation of parity violation in atomic ytterbium *Nat. Phys.* **15** 120–3
[44] Mariotti E *et al* 2014 Francium trapping at the INFN-LNL facility *Int. J. Mod. Phys.* E **23** 1430009
[45] Cahn S B, Ammon J, Kirilov E, Gurevich Y V, Murphree D, Paolino R, Rahmlow D A, Kozlov M G and DeMille D 2014 Zeeman-tuned rotational level-crossing spectroscopy in a diatomic free radical *Phys. Rev. Lett.* **112** 163002
[46] Williams S R, Jayakumar A, Hoffman M R, Blinov B B and Fortson E N 2013 Method for measuring the $6S_{1/2} \leftrightarrow 5D_{3/2}$ magnetic-dipole-transition moment in Ba^+ *Phys. Rev.* A **88** 012515
[47] Nuñez Portela M *et al* 2014 Ra^+ ion trapping: toward an atomic parity violation measurement and an optical clock *Appl. Phys.* B **114** 173–82
[48] Antypas D and Elliott D S 2013 Measurement of a weak transition moment using two-pathway coherent control *Phys. Rev.* A **87** 042505
[49] Sato T *et al* 2014 Development of francium atomic beam for the search of the electron electric dipole moment *EPJ Web Conf.* **66** 05019
[50] Gould H 2013 *private communication*
[51] Kuchiev M Y and Flambaum V V 2002 QED radiative corrections to parity nonconservation in heavy atoms *Phys. Rev. Lett.* **89** 283002
[52] Milstein A I, Sushkov O P and Terekhov I S 2002 Radiative corrections and parity nonconservation in heavy atoms *Phys. Rev. Lett.* **89** 283003
[53] Gomez E, Aubin S, Orozco L A, Sprouse G D, Iskrenova-Tchoukova E and Safronova M S 2008 Nuclear magnetic moment of ^{210}Fr: a combined theoretical and experimental approach *Phys. Rev. Lett.* **100** 172502
[54] Roberts B M and Ginges J S M 2020 Nuclear magnetic moments of francium-207–213 from precision hyperfine comparisons *Phys. Rev. Lett.* **125** 063002
[55] Ginges J S M and Volotka A V 2018 Testing atomic wave functions in the nuclear vicinity: the hyperfine structure with empirically deduced nuclear and quantum electrodynamic effects *Phys. Rev.* A **98** 032504
[56] Zhang J *et al* 2016 Efficient inter-trap transfer of cold francium atoms *Hyperfine Interact.* **237** 150
[57] Bennett S C and Wieman C E 1999 Measurement of the $6S \rightarrow 7S$ transition polarizability in atomic cesium and an improved test of the standard model *Phys. Rev. Lett.* **82** 2484–7
[58] Toh G, Damitz A, Tanner C E, Johnson W R and Elliott D S 2019 Determination of the scalar and vector polarizabilities of the cesium $6s^2S_{1/2} \rightarrow 7s^2S_{1/2}$ transition and implications for atomic parity nonconservation *Phys. Rev. Lett.* **123** 073002
[59] Collister R, Zhang J, Tandecki M, Aubin S, Gomez E, Gwinner G, Orozco L A, Pearson M R and Behr J A 2016 Photoionization of the francium $^7P_{3/2}$ state *Can. J. Phys.* **95** 234–7
[60] Vieira D J and Wieman C E 1992 *Parity nonconservation measurements of trapped radioactive isotopes — a precise test of the Standard Model* Research proposal *1303* Los Alamos Meson Physics Facility